Geoderma 167-168 (2011) 319–327

Contents lists available at SciVerse ScienceDirect

Geoderma

journal homepage: www.elsevier.com/locate/geoderma

Bauxitisation of anorthosites from Central Brazil

Fábio Soares de Oliveira [a,b,*], Angélica Fortes Drummond Chicarino Varajão [a], César Augusto Chicarino Varajão [a], Bruno Boulangé [c], Newton Souza Gomes [a]

[a] Departamento de Geologia, Universidade Federal de Ouro Preto, Campus Morro do Cruzeiro, s/n, Ouro Preto, 35400-000 MG, Brazil
[b] Instituto de Geociências, Departamento de Geografia, Universidade Federal de Minas Gerais, Av. Antônio Carlos, 6627, Belo Horizonte, 31270-901 MG, Brazil
[c] Museé de la Bauxite, Tourves, France

ARTICLE INFO

Article history:
Received 18 March 2011
Received in revised form 5 September 2011
Accepted 11 September 2011
Available online 5 November 2011

Keywords:
Bauxite
Alitisation
Isalteritic transformation
Anorthosite
Barro Alto Complex

ABSTRACT

Petrological studies using X-ray diffraction (XRD), X-ray fluorescence (XRF), optical microscopy, scanning electron microscopy (SEM-EDS) and electron microprobe analyzer (WDS) showed the mineralogical, micromorphological and geochemical transformations due to the bauxitisation of anorthosite from the Barro Alto Stratiform Mafic–Ultramafic Complex (Central Brazil). The hydrolytic alteration of the anorthosite occurred in two different stages in accordance with the order of stability of the minerals to the weathering: firstly the bytownite and secondly the ferromagnesian minerals. The weathering solutions, benefited from the existing network of fractures, percolated the weakness zones of the minerals characterising the microsystem of contact in which cores of plagioclase and ferromagnesian minerals were formed. In the first stage, the plagioclases are altered directly to gibbsite, and at an early stage, during the change process, the gibbsite crystals surround the primary ferromagnesian minerals that are totally or partially preserved. The transformation is isalteritic and is responsible for formation of porous alteromorphs consisting of septa of coarse gibbsite and fine gibbsite. As the weathering process advances, the ferromagnesian minerals directly enter to goethite. The boxworks of gibbsite and goethite characterise a primary plasmic microsystem.

1. Introduction

The history of the discovery and development of Brazilian bauxite (Melfi, 1997) reveals that most geological studies conducted thus far have concentrated on the Amazon region, which holds the largest reserves of bauxite, and on the southeastern and southern regions of Brazil. These lateritic deposits are formed due to the hydrolytic alteration of different rock types and exhibit different morphological and structural features.

In all, Brazil's reserves of bauxite approximate 3.8 billion tonnes and represent 10.6% of the global reserves (IBRAM, 2010). The northern region contains the largest reserves and accounts for approximately 95% of all Brazilian bauxite. The remaining 5% is located in the southeastern and southern regions of Brazil. Recently, in 1999, large deposit of bauxite was discovered in the midwestern region of Brazil, in the state of Goiás (Oliveira et al., 2009; Reis, 2007; Veiga and Girodo, 2008), precisely in the region of Barro Alto. This deposit that constitutes a reserve of nearly 160 million tonnes has developed from the anorthosites of the Superior Series of the layered mafic–ultramafic complex of Barro Alto (CBA), Neoproterozoic Brasília Belt, Tocantins Province (Almeida et al., 1981). Despite the bauxite reserves from the anorthosites in Port Loko, Sierra Leone (Hains, 2005), the process of bauxitisation from this rock has not yet been described, which further increases the scientific and economic interest of our pioneering study. Several recognised works have discussed bauxite originating from rocks such as syenite in the Loos Islands District (Guinea), Poços de Caldas and Passa Quatro (Brazil) and in Arkansas (USA). Until now, studies focused on the weathering of anorthosites only showed the formation of kaolinitic clay deposits such as in Malawi (Ministry of Energy and Mines of Malawi, 2009) and in the state of Rio Grande do Sul, Brazil (Formoso and Pintaude, 1978; Schenato and Formoso, 1993). From this standpoint, our study aims to characterise the formation process of bauxite from the anorthosites of the CBA, in the midwestern region of Brazil, and emphasise the major mineralogical, geochemical and micromorphological changes involved.

2. Materials and methods

The Barro Alto bauxite massif is located between the municipalities of Barro Alto and Santa Rita do Novo Destino in the state of Goiás, midwestern region of Brazil (Fig. 1A). The regional geomorphology is composed of three groups of mountain ranges: Santa Barbara, Laguna and Grande (Fig. 1C). Serra Grande is located in the bauxite

* Corresponding author at: Departamento de Geologia, Universidade Federal de Ouro Preto, Campus Morro do Cruzeiro, s/n, Ouro Preto, 35400-000 MG, Brazil. Tel.: +55 31 35517030; fax: +55 31 35591606.
E-mail address: fabio@ifmg.edu.br (F.S. de Oliveira).

0016-7061/$ – see front matter © 2011 Elsevier B.V. All rights reserved.
doi:10.1016/j.geoderma.2011.09.006

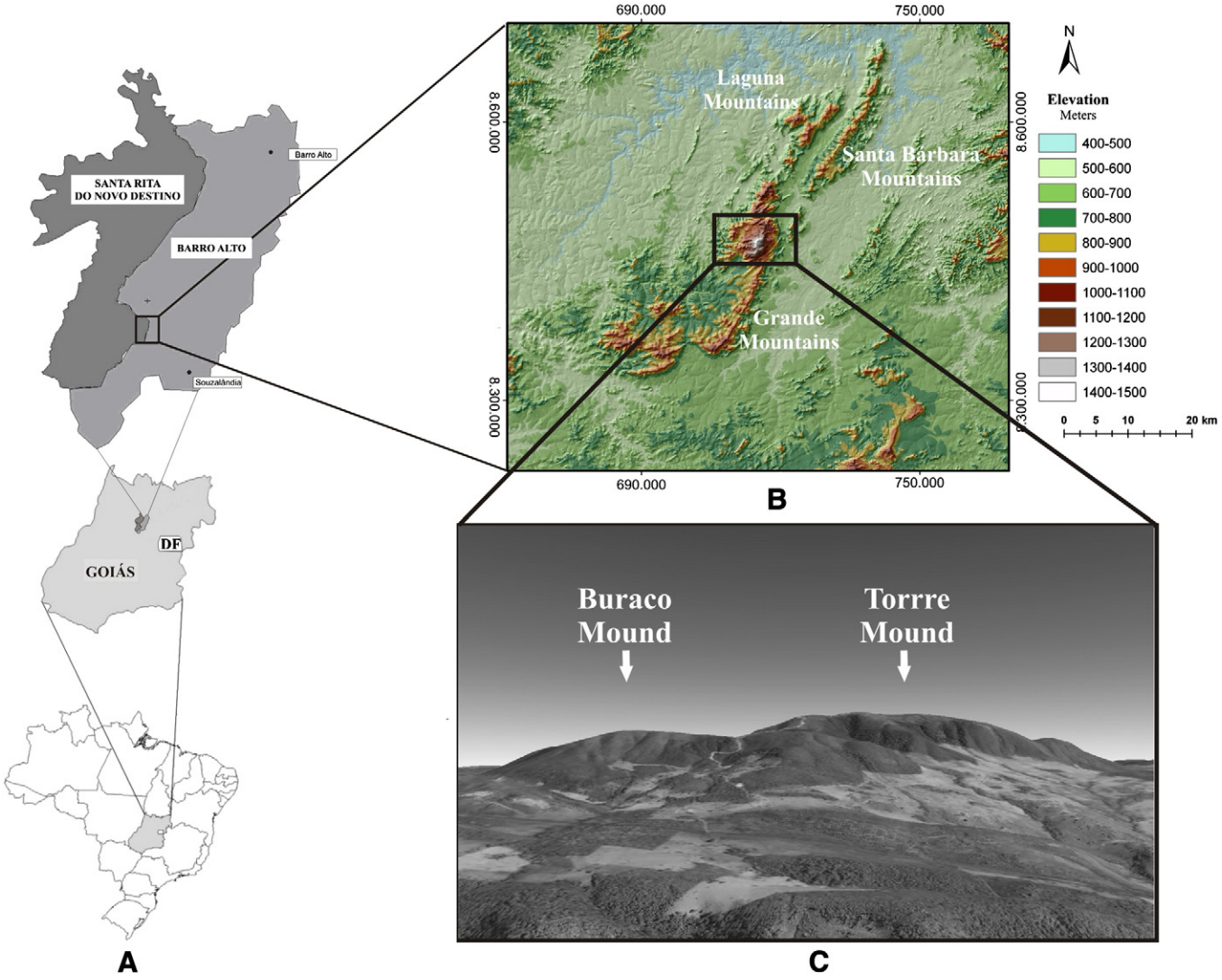

Fig. 1. A: The geographical location of the study area. B: The Digital Elevation Model of the CBA generated from the SRTM data showing the mountains of Santa Barbara, Laguna and Grande and the Bauxite Massif of Barro Alto; C: An image from Google Earth (with 2× vertical zoom) showing the Morro da Torre and the Morro do Buraco.

massif and is compartmentalised into two mountains known as Morro da Torre and Morro do Buraco. These two mountains have altitudes of 1500 m and 1300 m, respectively, which contrast with the surrounding morphology, which vary between 550 m and 900 m (Fig. 1B).

The climate in this region is tropical, with an average annual rainfall of 1600 mm. The vegetation consists of Cerrado fields (Radam-Brasil, 1981), which are preserved at elevations above 1000 m but are uncharacteristic in the lowlands with agricultural activity. The geology of the area is constituted by anorthosites that are geologically connected to gabbros rocks in the north and northwest and ultramafic rocks (serpentinite, dunite, harzburgite and pyroxenite) in the southeast (Correia et al., 2007; Ferreira Filho, 1998; Fuck et al., 1989).

After a systematic survey of the regolith through the macromorphological characterisation of lateral distributions and faciologic variations (Oliveira et al., 2009), 8 samples of fresh anorthosite, 25 samples of bauxite and 7 samples of the contact between the anorthosite and the bauxite (containing both materials) were collected for this study.

The chemical analysis was performed using X-ray fluorescence (XRF — Magix (PANalytical Philips spectrometer with a PW2540 autosampler)) on the bauxite and anorthosite samples. The following elements were analysed: Na, K, Mn, Mg, Ca, Fe, Al, Ti, P and Si, and the oxide contents were reported (in wt.%).

Mineralogical compositions of the powder of the same chemically analysed samples were obtained through X-ray diffraction (XRD) using an X'Pert Panalytical diffractometer with CuKα radiation in the range of 2° to 70° 2θ and a speed of 0.6°/min. The XRD patterns were interpreted using HighScore X'Pert Plus software and known literature patterns (Brindley and Brown, 1980). In addition, bulk density and mass balance analyses were obtained according Millot and Bonifas (1955).

Optical microscopic investigations were carried on 19 thin sections of undisturbed samples using a Zeiss trinocular optical microscope (Axiophot model) with an integrated digital camera. The concepts of Stoops et al. (1979) and Delvigne (1998) were used for the micromorphological descriptions.

The most representative sites were selected for morphological and chemical aspects using a scanning electron microscope (SEM, JOEL JSM-5510) coupled with an energy dispersive system (EDS). The elemental composition of the sites was obtained using an electron probe microanalyser (JOEL JCXA-8900 RL) operated with an acceleration potential of 15 kV and a current of 20 nA. The collection standards Ian Steele were used, except for Ti, which was collected using the rutile by Astimex collection. The following elements were determined in the microchemical analysis: Na, K, Mn, Mg, Ca, Fe, Al, Ti and Si. The oxide contents were reported (in wt%). The structural formula of the minerals was calculated using the MinPet 2.02 programme (Richard, 1995).

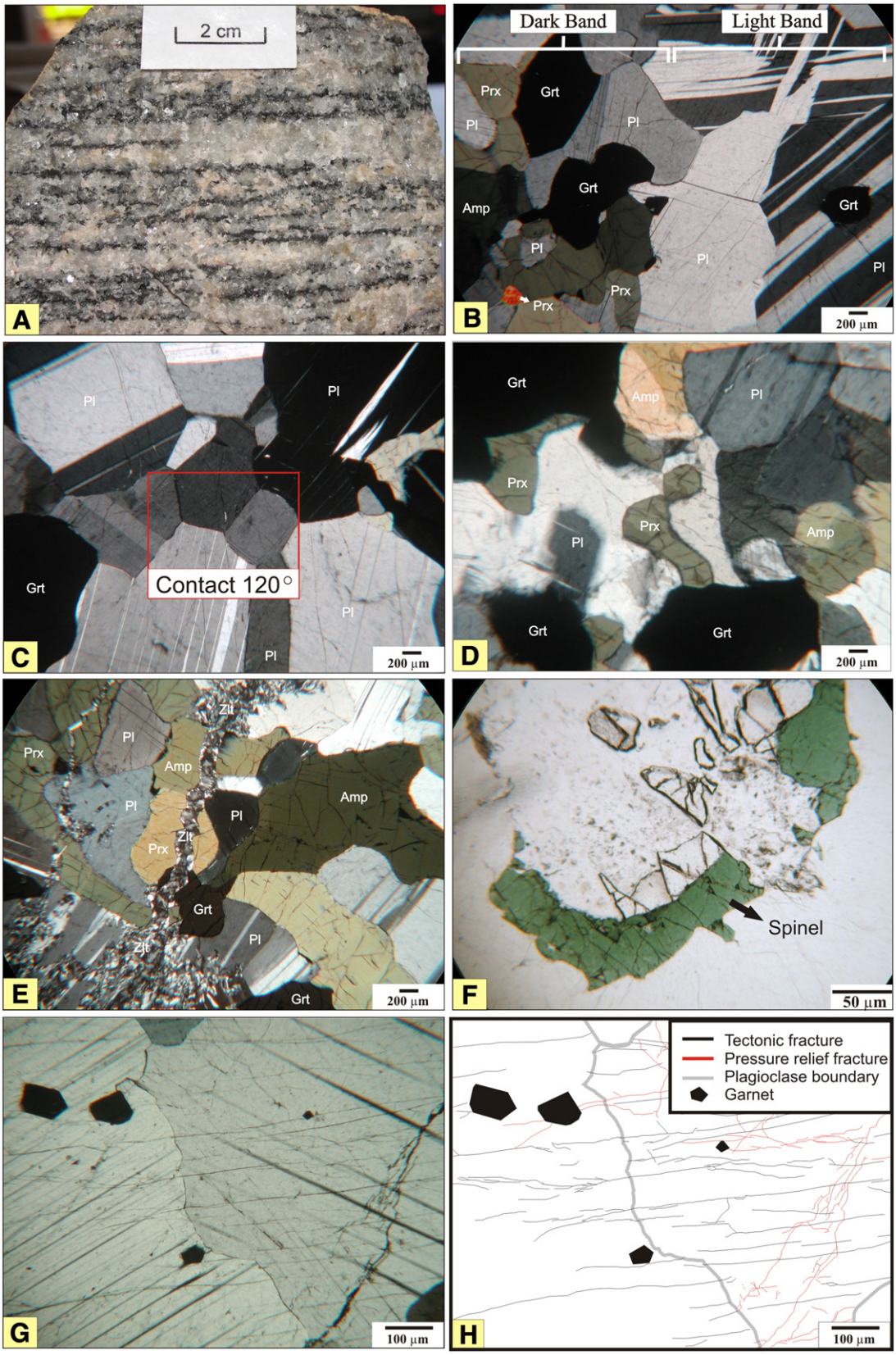

Fig. 2. A: Macroscopic view of anorthosite showing alternating light and dark bands. B: XPL (Optical microscope photomicrograph with crossed polarised light) of the contact between the clear band and the dark band of anorthosite. The photomicrograph highlights in the clear bands the presence of minerals Pl and Grt and, in the dark bands, the minerals Pl, Grt, Amp and Prx. C: XPL of the clear band of anorthosite highlighting the presence of Pl, Grt and its granoblastic polygonised texture. D: XPL of the dark band of anorthosite highlighting the presence of Pl, Grt, Amp and Prx. E: XPL of the dark band of anorthosite highlighting the presence of Pl, Grt, Amp, Prx and Zlt. F: XPL of the dark band of anorthosite, highlighting the presence of Spinel. G: XPL of plagioclase crystals that are intensely fractured in both directions. H: Schematic representation of tectonic fractures (drawn from Fig. 2G) and of the relieving pressure on plagioclase. Grt = Garnet; Pl = Plagioclase; Amp = Amphibole; Prx = Pyroxene; Zlt = Zeolite.

3. Results and discussion

3.1. The anorthosite

Macroscopically, the anorthosite is characterised as a holocrystalline, inequigranular and medium to coarse-grained leucocratic rock. Its colour varies from grey to light pink. The structure of the anorthosite is characterised by alternating light and dark bands with diffuse inter-band contact (Fig. 2A). The light bands, containing dispersed dark crystals, are prevalent and exhibit thicknesses ranging from 0.5 cm to 10 cm. The dark bands are discontinuous and exhibit thicknesses between 0.3 cm and 3.0 cm.

The alternation of light and dark bands is also visible microscopically (Fig. 2B). The light bands are primarily composed of plagioclase without preferential orientation, with fine to coarse grains making up approximately 95% of the mineralogical composition (Fig. 2C). These crystals show typical polysynthetic twinning with multiple albite, pericline and, to a lesser extent, Carlsbad. Microprobe analyses revealed a homogeneous chemical composition for the plagioclases, where the CaO content was approximately 15% and the Na_2O did not exceed 3% (Table 1). Chemically, the plagioclases were classified as bytownite, with an anorthite content of 77.4% (Deer et al., 1992). The contents of Al_2O_3, SiO_2 and FeO were 32.5%, 49.17% and 0.07%, respectively. No chemical zoning was observed in these crystals (the CaO content was constant towards the edge → centre → edge), indicating the metamorphic nature of the crystals. The mafic bands that were scattered through the light bands (5%) were either garnets surrounded by bytownite crystals or their inclusions (Fig. 2B and C).

The dark bands (Fig. 2D and E) are composed mainly of garnet (30%), amphibole (25%), clino- and orthopyroxene (20%) and plagioclase (20%), along with accessory and secondary minerals (<5%). Garnets are chemically made up of 40.4% almandine, 40.4% pyrope, 18% grossular and 1.2% sperssartite (Table 1). The amphiboles exhibit a brownish-green hue and are generally classified as pargasitic hornblende (Leake et al., 1997). The composition of clinopyroxene is between that of augite and diopside, and it forms crystals measuring up to 2 mm. On the other hand, orthopyroxene occurs as prismatic crystals with pleochroism, exhibits pale-green to brownish and yellowish hues and is chemically classified as hypersthene. The accessory minerals (<5%) are spinel and titanites. The spinels exhibit a bottle-green colour in plane polarised light (Fig. 2F) and are chemically classified as a pleonaste that is between *stricto sensu* spinel and hercynite because to the similarity in the proportions of Fe and Mg (Deer et al., 1992). Titanite is rare (<1%) and forms small euhedral crystals that can only be observed optically. Fractures that intercept the light and dark bands may occasionally be filled by secondary minerals such as zeolites. Given the high levels of Ca (Table 1), these zeolites were classified as laumontite. The abrupt contact of the zeolite with mafic minerals and the diffuse contact with the plagioclase suggest that zeolite is the product of the changes of plagioclase under hypogenous environment (Fig. 2E). The paragenesis of the mafic mineral assemblage indicates a high degree of metamorphism in the granulite facies, mainly due to the presence of orthopyroxene and spinel (Vernon and Clarke, 2008) from igneous protoliths, with subsequent retrogressive metamorphism that is indicated by the presence of amphibole and zeolite.

The texture of the rock is granoblastic polygonised, in which the crystals exhibit contacts in parallel faces with angles of 120° (Fig. 2C). Features of deformation, such as twinned minted, undulatory extinction and subgrains, are recognised. Furthermore, the rock is heavily fractured and two groups of fractures are recognised: (I) regular and parallel fractures and (II) irregular fractures that are sometimes positioned obliquely with respect to the first group (Fig. 2G and H). The first case suggests a source associated with compressive tectonic forces, whereas the second case suggests pressure relief that is probably related to decompression promoted by the erosion of the rocks overlying the intrusive body.

The XRF analysis of the anorthosite reflects their mineralogical composition (Table 2).

Table 1
Average composition (weight %) of selected minerals from the Barro Alto anorthosite obtained by electron microprobe and structural formulas of mineral phases. The standardisation of cations was based on the oxygen molecules, which numbered 34 for plagioclase, 12 for garnet, 23 for the amphibole, 6 for pyroxene and 32 for the spinel.

	Plagioclase	Garnet	Amphibole	Pyroxene		Spinel	Zeolite
				Clino	Orto		
Analyses	14	7	11	4	2	3	9
SiO_2	49.17 ± 0.37	40.34 ± 0.89	39.01 ± 0.37	44.77 ± 0.51	50.35 ± 0.22	0	47.30 ± 0.67
TiO_2	0.01 ± 0.01	0.07 ± 0.00	1.77 ± 0.18	1.08 ± 0.06	0.15 ± 0.01	0	0
Al_2O_3	32.50 ± 0.36	22.51 ± 0.45	16.98 ± 0.25	12.75 ± 0.70	1.14 ± 0.12	60.57 ± 0.52	26.09 ± 0.39
FeO	0.07 ± 0.03	19.24 ± 0.33	13.6 ± 0.31	8.87 ± 0.16	37.02 ± 0.20	26.63 ± 0.73	0.02 ± 0.01
MnO	0	0.57 ± 0.04	0.10 ± 0.03	0.1 ± 0.02	0.68 ± 0.06	0	0
MgO	0	10.8 ± 0.24	10.02 ± 0.19	8.71 ± 0.25	10.02 ± 0.32	12.78 ± 0.63	0
CaO	15.63 ± 0.34	6.67 ± 0.33	11.57 ± 0.13	22.13 ± 0.16	2.3 ± 0.13	0	13.04 ± 0.22
Na_2O	2.50 ± 0.17	0.01 ± 0.00	2.9 ± 0.06	1.10 ± 0.04	0.01 ± 0.00	0	0.33 ± 0.14
K_2O	0.03 ± 0.02	0.01 ± 0.00	0.32 ± 0.02	0.01 ± 0.00	0.01 ± 0.00	0	0.02 ± 0.01
Total	99.91	100.22	96.26	99.52	101.01	99.98	86.8

Cations (structural formula)

Si	8.99	TSi	3.02	TSi	5.87	TSi	1.67	TSi	1.97	Al	15.37
Al	7.00	Al^{VI}	1.98	TAl	2.12	TAl	0.32	TAl	0.03	Fe^2	4.80
Ti	0	Ti	0	CAl	0.88	M1Al	0.23	M1Al	0.02	Mg	4.10
Fe^2	0.01	Fe^2	1.20	CFe^3	0.14	M1Ti	0.03	M1Ti	0.01		
Mn	0	Mg	1.20	CTi	0.20	$M1Fe^2$	0.24	$M1Fe^2$	0.28		
Mg	0	Mn	0.03	CMg	2.25	M1Mg	0.48	M1Mg	0.58		
Ca	3.06	Ca	0.53	CFe^2	1.51	$M2Fe^2$	0.03	$M2Fe^2$	0.91		
Na	0.89	Na	0	CMn	0.006	M2Mn	0	M2Mn	0.01		
K	0.01	Almandine	40.4	BFe^2	0.05	M2Ca	0.88	M2Ca	0.09		
Albite	22.4	Grossular	18.0	BMn	0.006	M2Na	0.08	M2Na	0		
Anorthite	77.4	Pyrope	40.4	BCa	1.86	M2K	0	M2K	0		
Orthoclase	0.2	Spessartite	1.2	BNa	0.07						
				ANa	0.77						
				AK	0.06						

Table 2
Chemical composition (%) of anorthosite and bauxite, obtained by XRF, mass balance and chemical composition of gibbsite and goethite obtained by microprobe analysis.

	Anorthosite	Bauxite	Mass balance[1]	Gibbsite	Goethite
Samples/points	8	25	–	5	4
Bulk density (g/cm^3)	2.68	1.48	–	–	–
SiO_2	45.46 ± 0.43	0.77 ± 0.32	−99.06	0.00	0.00
TiO_2	0.10 ± 0.01	0.18 ± 0.07	−0.59	0.00	0.2 ± 0.08
Al_2O_3	33.90 ± 0.70	61.20 ± 1.36	−0.30	79.93 ± 0.15	19.80 ± 1.06
FeO	1.73 ± 0.33	3.13 ± 1.85	−0.08	0.00	62.35 ± 1.29
MnO	0.02 ± 0.03	<LQ[2]	−100	0.00	0.02 ± 0.01
MgO	0.76 ± 0.04	0.10 ± 0.04	−92.73	0.00	0.00
CaO	15.61 ± 0.44	<LQ	−100	0.00	0.14 ± 0.07
Na_2O	2.34 ± 0.27	<LQ	−100	0.00	0.02 ± 0.01
K_2O	0.03 ± 0.00	<LQ	−100	0.00	0.03 ± 0.01
P_2O_5	<LQ	0.03 ± 0.01	136.67	0.00	0.00
PPC	0.52 ± 0.10	34.0 ± 0.79	–	–	–
Total	100.47	99.41	–	79.93	82.56

[1] Negative values indicate loss of the element and positive values indicate gain of the element (Millot and Bonifas, 1955).
[2] LQ = Detection Limit = 0.01%.

3.2. The transformation of anorthosite into bauxite

Macroscopically and microscopically, the contact between anorthosite and bauxite is abrupt (Fig. 3A). Pre-existing fractures in the anorthosite allow the progress of the weathering front, which facilitates the percolation of the fluids and promotes the dissolution of the primary minerals and the subsequent mineralogical neoformations that occur in two phases. In the first phase, the plagioclases are altered directly to gibbsite, *i.e.*, without an intermediate phase, and in the second phase, ferromagnesian minerals are transformed into goethite, in accordance with the order of the stability of minerals (Goldich, 1938). At an early stage of the alteration process, the gibbsite crystals surround the primary ferromagnesian minerals that are totally or partially preserved (Fig. 3A). As the weathering process advances, these minerals directly transform into goethite. A comparison between the diffractograms of the anorthosite and the bauxite (Fig. 3B) shows an abrupt change between their mineralogical compositions, where the primary mineral assemblage is replaced by a secondary mineralogical composition.

In addition to the fractures, the weathering front also advances along the planes of weakness of the minerals (twinnings and cleavages) forming regular and irregular contours (Delvigne, 1998; Stoops et al., 1979). The advancement of this process is characterised by regular and linear crossed microsystems of contact, in which the cores of plagioclase and ferromagnesian are formed (Figs. 3C and 4D).

The cores of plagioclases are characterised by residual fragments that are surrounded by gibbsite, originated directly from the weathering of the plagioclases (Fig. 3C). They have quadratic to rectangular shapes and are separated by gibbsitic septa, which exhibits a direction of crystal growth perpendicular to the cores. Microprobe analyses from the core to the adjacent secondary material (Fig. 4A) indicate the following sequence: plagioclase → void → gibbsite. Punctual microanalysis in various cores of plagioclase (Fig. 4B) confirms that the residual presence of these minerals occurs without the existence of an aluminosilicate intermediate phase until their total consumption, which characterises the process of alitisation (Pedro, 1964). The space that separates the residual cores of plagioclase of gibbsite is described as a contact void (Nahon, 1991; Stoops, 2003). SEM images confirm these observations and emphasise the presence of fragments of plagioclase with surface of dissolution, gibbsite, and void (Fig. 4C). Clearly, the process of transformation of bytownite into gibbsite is associated with a relative accumulation of aluminium and leaching of the other chemical components, especially alkalis and silica.

Microchemical maps of the contact between anorthosite and bauxite in thin sections (Fig. 4D) show the relative accumulation of aluminium. This element presents a uniform distribution in the anorthosite, whereas in the bauxite, it undergoes a marked redistribution of local concentrations that correspond to the gibbsitic septa. The levels of Si, Ca and Na in bauxite exhibit a clear reduction. A few concentration of Si in the bauxite are restricted to the ferromagnesian minerals that have not undergone complete change.

The ferromagnesian minerals also exhibit the formation of isolated residual cores from primary mineral that are directly transformed into goethite (Fig. 3D). As in the case of the plagioclase, the intermediate mineral phase does not occur here. Goethite halos are formed around the residual cores and are separated by voids. Similar observations were made by Embrechts and Stoops (1982). The complete alteration of ferromagnesian minerals occurs when the plagioclases were totally transformed into gibbsite. Therefore, no significant dispersion of iron is observed; this fact is considered justification for the white and red spotted coloration of the newly formed bauxites.

The boxworks of gibbsite and goethite are formed upon the completion of the alteromorphs of primary minerals, generating an isalteritic fabric. This structure is characterised by a crystaliplasma comprising a network of gibbsite boxworks, which involve the boxworks of goethite (Fig. 5A). This is the primary plasmic microsystem (Delvigne, 1998).

The voids in the newly formed bauxite are abundant (Fig. 5B) and are derived from the total consumption of residual cores of primary minerals. They exhibit dimensions ranging from millimetres to centimetres and shapes ranging from rectangular to quadratic. Irregular, amoeboidal voids may also occur, but in smaller proportions.

The newly formed porous bauxite comprises approximately 79.93% Al_2O_3 (Table 2). The gibbsites organised in septa (Fig. 5C and D) are predominant and account for approximately 90% of the total mineralogical composition. Both macro and microcrystals of gibbsite coexist and are distributed such that the microcrystals are concentrated in the central parts of the septa and the macrocrystallisation appears at the edges (Fig. 5E). The distribution features two generations of hydroxides crystals of aluminium. The gradual transition between the two generations indicates their co-geneticity, which suggests that macrocrystallisation represents the growth of the crystal network of gibbsite in the direction of the source of aluminium, *i.e.*, the cores of plagioclases (Nahon, 1991).

The goethites (Fig. 5F and G), which make up approximately 5% to 10% of the total mineralogical composition, are primarily concentrated in the dark bands. They exhibit fine granulometry, contain high levels of aluminium (which isomorphically replaces the iron) and are chemically classified as aluminium goethites. The average composition is 62.35% Fe_2O_3 and 19.80% Al_2O_3 (Table 2), which is attributed to the high availability of aluminium in its environment of formation and in the associated minerals such as garnet.

The overall chemical composition of porous bauxite (Table 2) reflects its mineralogical composition, which exhibits high Al_2O_3 content

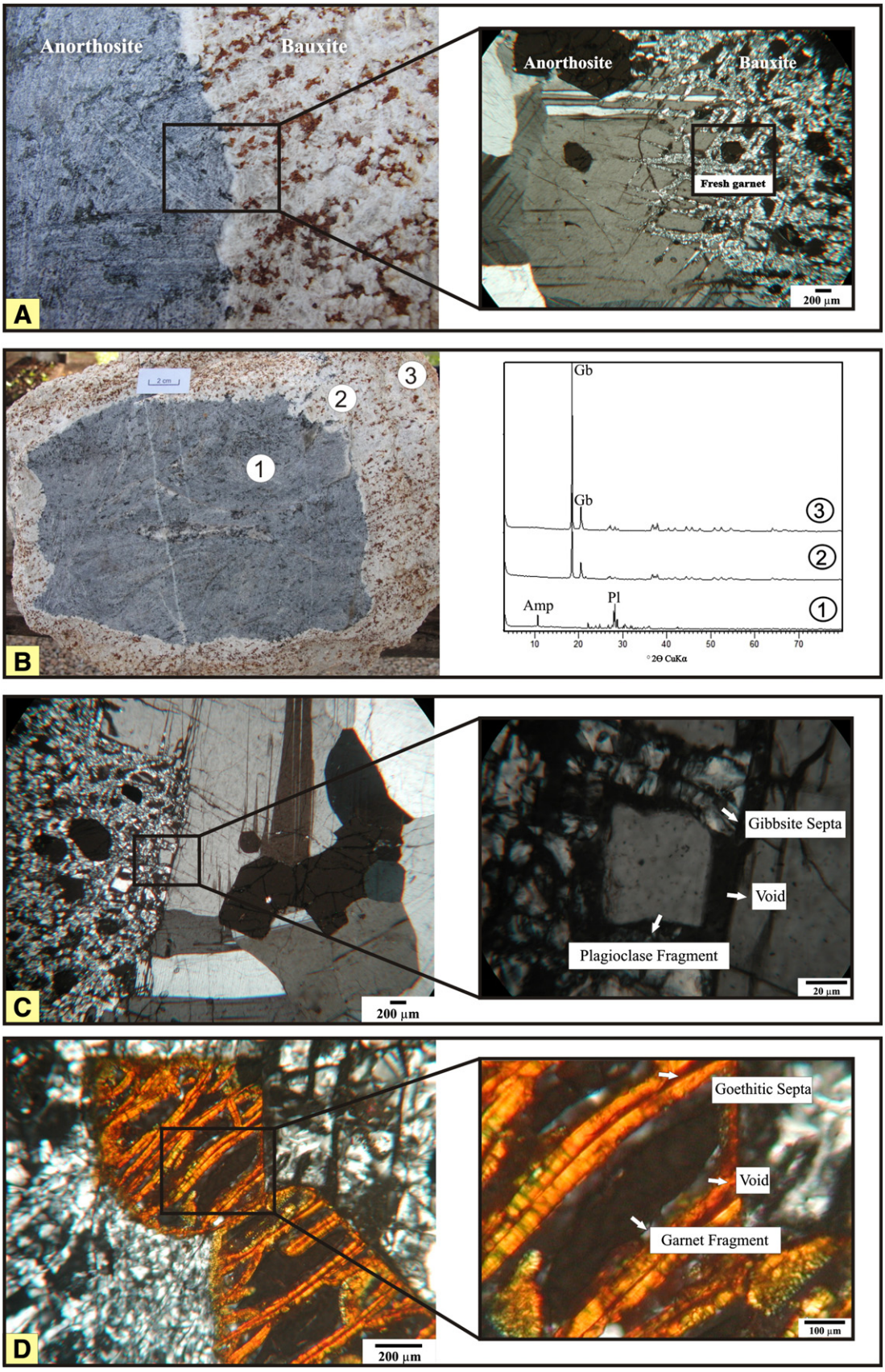

Fig. 3. A: Macroscopic aspect of the abrupt contact between anorthosite and bauxite with microscopic detail indicating the presence of unweathered crystals of garnet surrounded by gibbsite. B: X-ray diffraction patterns (Cukα radiation) of the transition between the anorthosite and the bauxite showing the abrupt mineralogical change of bytownite into gibbsite. Pl: Plagioclase, Amp: Amphibole, Gb: Gibbsite. C: XPL with the SEM of fragments of plagioclase, void and gibbsitic septa. D: XPL with the SEM showing the presence of residual fragments of garnet, voids and goethitic septa.

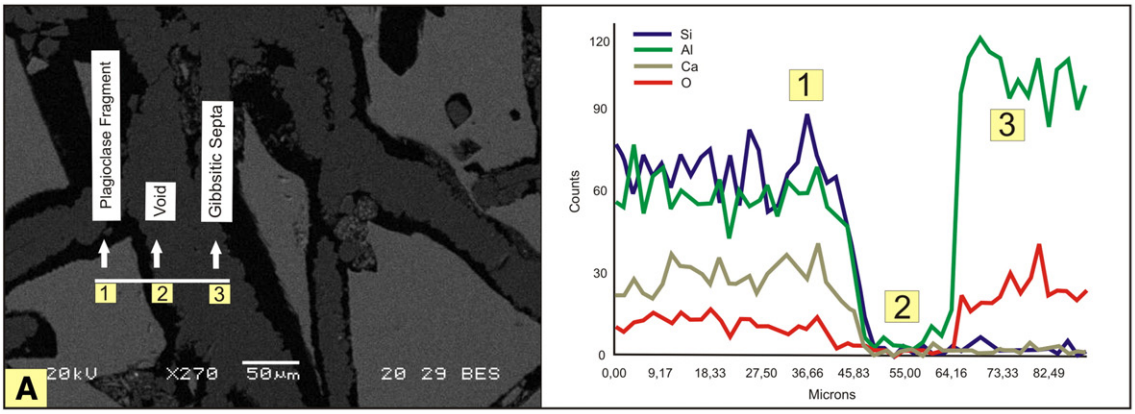

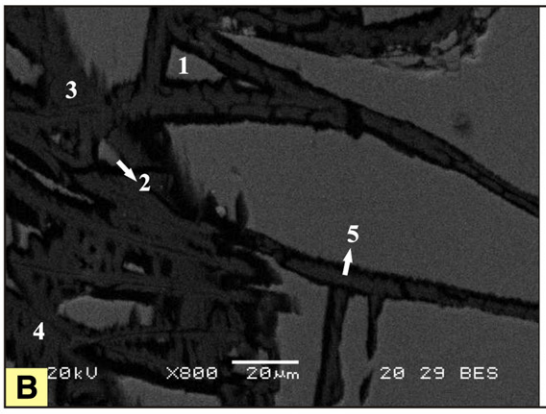

	1	2	3	4	5
SiO_2	48,76	48,67	0	0,01	0,01
TiO_2	0	0	0,02	0,02	0,01
Al_2O_3	32,45	32,48	77,76	72,18	79,63
FeO	0,08	0,14	-	-	-
Fe_2O_3	-	-	0,47	0,24	0,26
MnO	0	0,04	0	0,01	0
CaO	15,74	15,65	0,07	0,07	0,05
Na_2O	2,43	2,39	0	0,03	0,01
K_2O	0,07	0,08	0	0	0
Total	**99,53**	**99,45**	**78,32**	**72,56**	**79,97**

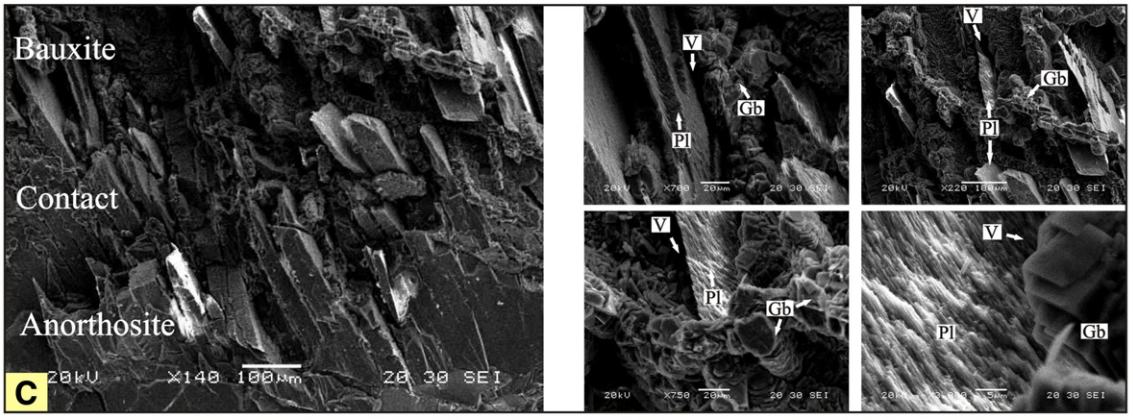

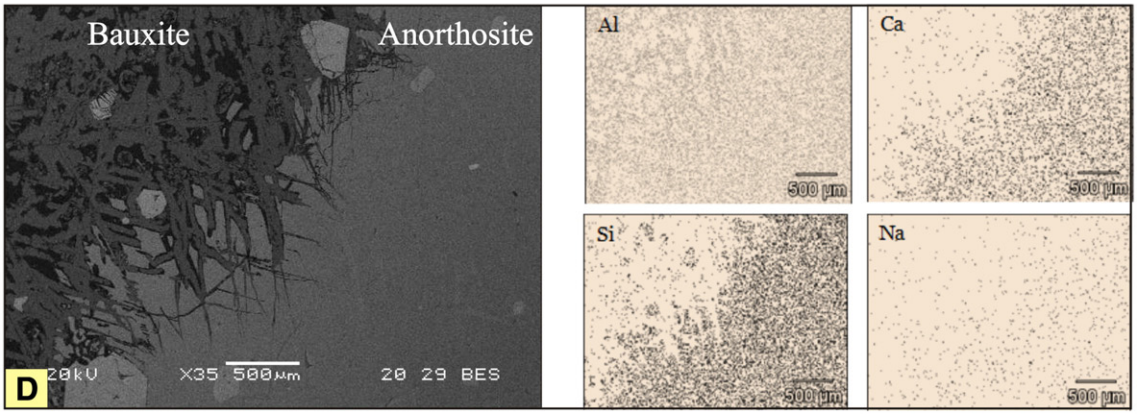

Fig. 4. A: SEM from thin section showing fragments of plagioclase surrounded by gibbsitic septa with its respective microprobe line indicating the distribution of Si, Al, Ca and O. B: SEM from thin section showing fragments of plagioclase surrounded by gibbsitic septa with their specific microprobe analysis. C: SEM from fragment of the contact between anorthosite and bauxite. In detail note the presence of plagioclase surrounded by gibbsitic septa and separated from each other by voids. P: void, GB: gibbsite, Pl: plagioclase. D: Microchemical maps of the Al, Si, Ca and Na elements at the contact between anorthosite and bauxite obtained using EDS. The dark spots on the image indicate the distribution of the chemical elements.

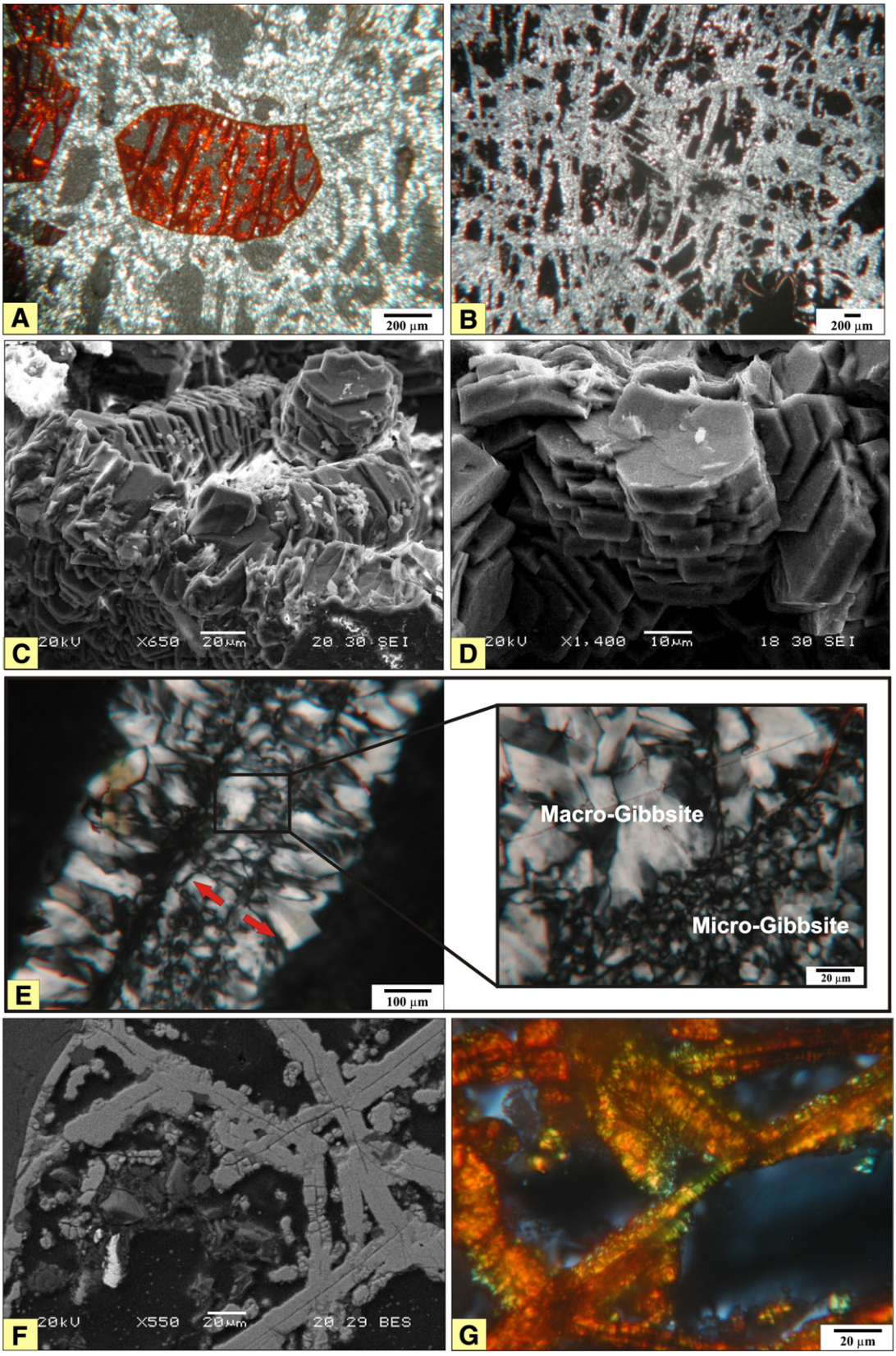

Fig. 5. A: XPL of the crystaliplasma gibbsite involving skeletons of goethite box works. B: XPL indicating the high porosity of the isalteritic bauxite with the predominance of regular voids. C: SEM of the septa of the gibbsite network. D: SEM of the gibbsite septa showing the packing crystals of the gibbsite. E: XPL of the gibbsite septa highlighting the growth of crystals in the opposite direction and the presence of macro and microcrystals of co-genetic gibbsite. F: SEM of the goethitic septa. G: XPL of the goethitic septa.

(61.20% on average) and low concentrations of Fe_2O_3 and SiO_2 (3.13% and 0.77%, respectively). In the case of Si, the levels are most likely related to the presence of small residual fragments of ferromagnesian minerals.

The isalteritic structure of the porous bauxite, which characterises an isovolumetric alteration from the anorthosite, when correlated to the bulk density of anorthosite (2.68 g/cm^3) and of the porous bauxite (1.48 g/cm^3) shows a relative concentration of Al in the porous bauxite and an almost total loss of silica and alkalis (Table 2).

4. Conclusions

- Anorthosite is the potential rock generator of Barro Alto bauxite. Its mineralogical composition is predominantly plagioclase (bytownite) with smaller amounts of garnets, amphibole, pyroxene (clino and ortho), accessory minerals (spinel and titanite) and the secondary mineral zeolite. Its mineralogical paragenesis, along with its granoblastic texture indicates that the igneous protolith, had undergone a high degree of metamorphism (indicated by the presence of spinel and orthopyroxene) and retrogressive metamorphism (indicated by the presence of zeolite and hornblende).
- In the supergene environment, the anorthosites were altered by weathering solutions that percolated the zones of weakness of the minerals and were initially benefitted from the existing network of fractures. The origin of these fractures is related to tectonic events and pressure relief.
- The process of bauxitisation occurred in two stages. The first stage involved the transformation of bytownite into gibbsite and the second step involved the transformation of ferromagnesian minerals into goethite. The mineral phases of intermediate chemical composition, *i.e.*, aluminosilicates or iron silicates, were not observed, which indicates a typical alitisation process.
- The bauxite formed by the direct alteration of anorthosite is porous and whitish, indicating little dispersion of Fe. It is characterised by a gibbsitic crystaliplasma that involves the skeletons of ferromagnesian minerals, which is alteromorphosed by the goethite boxworks. The alteromorphosis of the primary minerals configures the isalteritic fabric and isovolumetric alteration, whereas the direct loss of alkalis and silica reflects the process of the relative accumulation of aluminium.

Acknowledgements

The authors thank CNPq (Conselho Nacional de Desenvolvimento Científico e Tecnológico) and CAPES (Coordenação de Aperfeiçoamento de Pessoal de Nível Superior) for financial support. We are grateful to EDEM (Empresa de Desenvolvimento em Mineração e Participações Ltda) for financial support and field assistance providing analysis and samples.

References

Almeida, F.F.M., Hasui, Y., Brito Neves, B.B., Fuck, R.A., 1981. Brazilian structural provinces: an introduction. Earth-Science Reviews 17, 1–29.
Brasil, Ministério das Minas e Energia, Departamento Nacional da Produção de Minerais, Projeto RADAMBRASIL, 1981. Folhas SC.22 e SD.22: geologia, geomorfologia, pedologia, vegetação e uso potencial da terra. Rio de Janeiro, v.22 e 25, 524 pp.
Brindley, G.W., Brown, G., 1980. Crystal Structures of Clay Minerals and Their X-ray Identification (Monograph 5). Min. Soc., London. 495 pp.
Correia, C.T., Girardi, V.A.V., Basei, M.A.S., Nutman, A., 2007. Cryogenian U–Pb (SHRIMP I) zircon ages of anorthosites from the upper sequences of Niquelândia and Barro Alto Complexes, Central Brazil. Revista Brasileira de Geociências 37, 70–75.
Deer, W.A., Howie, R.A., Zussman, J., 1992. An Introduction to the Rock-Forming Minerals, 2nd ed. Pearson, New York. 696 pp.
Delvigne, J.E., 1998. Atlas of Micromorphology of Mineral Alteration and Weathering, 3rd ed. Canadian Mineralogist Special Publication. 509 pp.
Embrechts, J., Stoops, G., 1982. Microscopical aspects of garnet weathering in a humid tropical environment. Journal of Soil Science 33, 535–545.
Ferreira Filho, C.F., 1998. Geology and petrology of the large layered intrusions of central Brazil: implications for PGE mineralization. Platinum Symposium, Rustemburg, South Africa, pp. 107–110.
Formoso, M.L.L., Pintaude, D.A., 1978. Estudo da alteração do anortosito de Capivarita, Rio Pardo, RS. Revista Brasileira de Geociências 8, 180–205.
Fuck, R.A., Brito Neves, B.B., Cordani, U.G., Kawashita, K., 1989. Geocronologia Rb–Sr no Complexo Barro Alto, Goiás: evidência de metamorfismo de alto grau e colisão continental há 1300 Ma no Brasil Central. Geochimica Brasiliensis 3, 125–140.
Goldich, S.S., 1938. A study in rock weathering. Journal of Geology 46, 17–58.
Hains, D.H., 2005. Competent person's report on Port Loko bauxite deposit in Sierra Leone. http://www.moydow.com/AIM_Rule26/CPR_Port_Loko.pdf2005.
IBRAM (The Brazilian Mining Association), 2010. Information and Analysis of the Brazilian Mineral Economy, 5th ed. IBRAM, Brasília. 9 pp.
Leake, B.E., Wooley, A.R., Hawthorne, F.C., Kato, A., Krivovichev, V.G., Laird, J., Maresch, W.V., Schumacher, J.C., Stephenson, N.C.N., Wittaker, E.J.W., Youzhi, G., 1997. Nomenclature of amphibols of the Internacional Mineralogical Association Comission on New Minerals and Mineral Names. Mining Magazine 61, 295–321.
Melfi, A.J., 1997. Brazilian bauxite deposits: a review, In: Carvalho, A., Boulangé, B., Melfi, A.J., Lucas, Y. (Eds.), Brazilian Bauxites, 1st ed. USP/FAPESP/ORSTOM, São Paulo, pp. 3–22.
Millot, G., Bonifas, M., 1955. Transformations isovolumetriques dans les phenomenes de laterisation et de bauxitisation. Bulletin Service Carte Géolique d'Alsace et Lorraine 8, 3–20.
Ministry of Energy and Mines of Malawi, 2009. Mineral Potential of Malawi. http://www.bgs.ac.uk/downloads/start.cfm?id=12422009.
Nahon, D.B., 1991. Introduction to the Petrology of Soils and Chemical Weathering. John Wiley & Sons, New York. 313 pp.
Oliveira, F.S., Varajão, A.F.D.C., Varajão, C.A.C., Boulangé, B., Costa, J.L.G., Vessani, L.A., 2009. Alteração supergênica e morfogênese tropical no Complexo Máfico-Ultramáfico Acamadado de Barro Alto, GO. Geoc., 28, pp. 255–272.
Pedro, G., 1964. Contribution à l'étude expérimentale de altération chimique dês roches cristallines. PhD Thesis, Faculté des Sciences Paris, Paris, 344 pp.
Reis, L.G.R., 2007. Goiás: investimentos em novos projetos superam US$ 2 bilhões. Ver. Bras. Min., 258, pp. 28–37.
Richard, L.R., 1995. Minpet: Mineralogical and Petrological Data Processing System, Version 2.02. Minpet Geological Software, Quebec, Canada.
Schenato, F., Formoso, M.L.L., 1993. Aspectos mineralógicos e geoquímicos da alteração do Anortosito Capivarita, RS. Geochimica Brasiliensis 7, 1–17.
Stoops, G., 2003. Guidelines for Analysis and Description of Soil and Regolith Thin Sections. Soil Science Society of America, Madison, Wisconsin. 184 pp.
Stoops, G., Altemuller, H.J., Bisdom, E.B.A., Delvigne, J., Dobrosvolsky, V.V., FitzPatrick, E.A., Paneque, G., Sleeman, J., 1979. Guidelines for the description of mineral alterations in soil micromorphology. Pedologie 29, 121–135.
Veiga, A.T.C., Girodo, A.C., 2008. Modelamento geológico e abordagem geoestatística da jazida de bauxita de Barro Alto – GO, Brasil. Relatório Interno GEOS Consultoria. 157 pp.
Vernon, R.H., Clarke, G.L., 2008. Principles of Metamorphic Petrology. Cambridge University Press, Cambridge. 406 pp.